Structural Engineering and Mechanics, Vol. 44, No. 6 (2012) 815-837
DOI: http://dx.doi.org/10.12989/sem.2012.44.6.815

Improved interfacial stress analysis of a plated beam

Sheng-Wang Hao*, Yan Liu and Xiao-Dan Liu

School of Civil Engineering and Mechanics, Yanshan University, Qinhuangdao 066004, People's Republic of China

(Received March 21, 2012, Revised May 12, 2012, Accepted November 13, 2012)

Abstract. A plated beam is strengthened by bonding a thin plate to the tension face; it often fails because of premature debonding of the thin plate from the original beam in a brittle manner. A sound understanding of the mechanism of such debonding failure is very important for the effective use of this strengthening technique. This paper presents an improved analytical solution for interfacial stresses that incorporates multiple loading conditions simultaneously, including prestress, mechanical and thermal loads, and the effects of adherend shear deformations and curvature mismatches between the beam and the plate. Simply supported beams bonded with a thin prestressing plate and subjected to both mechanical and thermal loading were considered in the present work. The effects of the curvature mismatch and adherend shear deformations of the beam and plate were investigated and compared. The main mechanisms affecting the distribution of interfacial stresses were analyzed. Both the normal and shear stresses were found to be significantly influenced by the coupled effects of the elastic moduli with the ratios E_a/E_b and E_a/E_p.

Keywords: interfacial stress; debonding; beam; prestress; temperature; strengthening

1. Introduction

Strengthening beams of reinforced concrete (RC) and other materials by bonding a steel, fiber-reinforced polymer (FRP), or plastic plate to it has become a popular method because it is a simple and quick technique, and it also affords other advantages. This method glues a plate to the tension faces of beams. Its effectiveness depends on the bonding between the plate and the beam because debonding along the interface leads to premature failure of the structure.

The debonding mode of plated beams has been studied extensively (Roberts and Haji-Kazemi 1989, Malek *et al.* 1998, Smith and Teng 2001, Rasheed and Pervaiz 2002). Yao and Teng (2007) presented an experimental study on plate end debonding failures in FRP-plated RC beams. Maalej and Leong (2005) investigated the effect of the beam size and FRP thickness on the interfacial shear stress concentration and failure mode of FRP-strengthened beams based on an experimental research program. Ahmed *et al.* (2001) tested a series of RC beams strengthened with carbon fiber reinforced polymer (CFRP), and Fanning *et al*. (2001) presented the results of flexural tests on ten reinforced concrete beams strengthened with different plate configurations. Tests revealed that debonding failure is a common cause of brittle failure in beams strengthened with a plate (Jones *et al.* 1988,

*Corresponding author, Associate Professor, E-mail: haoshengwang@gmail.com

Swamy *et al.* 1989, Oehlers 1992, Arslan 2008). To investigate the structural behavior of reinforced concrete beams strengthened with adhesively bonded fiber reinforced polymer (FRP), Ascione and Feo (2000) conducted experimental and theoretical analyses using 2D nonlinear finite-element modeling incorporating a "damage" material model for concrete. Experimental investigations (Jones *et al.* 1988, Swamy *et al.* 1989, Oehlers 1992, Yao and Teng 2007, Arslan 2008, Maalej and Leong 2005, Garden *et al.* 1998, Etman *et al.* 2000, Ahmed *et al.* 2001, Fanning *et al.* 2001, Bonacci *et al.* 2001, Maalej *et al.* 2001, Schnerch *et al.* 2006, Ascione and Feo 2000, Saadatmanesh and Ehsani 1991) and numerical results (Täljsten 1997, Malek *et al.* 1998, Teng *et al.* 2002, Ziraba and Baluch 1995, Ascione and Feo 2000, Rahimi and Hutchinson 2001, Arduini *et al.* 1997) have provided significant insights into the behavior and failure mechanisms of a plated beam and have been very helpful in the development of predictive models.

Many researchers have made important contributions to debonding strength models (Oehlers 1992, Baluch *et al*. 1995, Raoof *et al*. 2000, Smith and Teng 2001, 2002a, b, Saadatmanesh and Malek 1998, Yuan *et al*. 2004, Gao *et al*. 2005). Roberts and Haji-Kazemi (1989) proposed an analytical solution based on partial interaction theory to predict the shear and normal stress concentrations in adhesive joints. Results from both theory and finite-element analysis (Täljsten 1997) on a beam with a strengthening plate bonded to its soffit and loaded with an arbitrary point load showed that the stresses were very large at the end of the plate but quickly diminished nearer to the center of the beam. Malek *et al*. (1998) provided a closed-form solution to calculate the stresses at the plate ends and investigated the effect of large flexural cracks along the beam. Rabinovich and Frostig (2000) provided a closed-form high-order analysis of reinforced concrete beams strengthened with FRP plates that satisfied the free-surface condition at the ends of the adhesive layer. Smith and Teng (2001), Yang *et al*. (2009) carried out a thorough review of these solutions, and the former presented a general solution based on the deformation compatibility approach, which seems to be a more widely applicable solution. Shen *et al*. (2001) developed a complementary energy method to study the interfacial stresses for simply supported RC beams and slabs bonded with a thin composite plate or steel plate. Based on the analysis by Smith and Teng (2001), Tounsi *et al*. (2006, 2009) developed an improved theoretical solution for interfacial stresses in concrete beams strengthened with FRP plate in which the adherend shear deformations are considered. Yang and Wu (2007) presented another improved solution for interfacial stresses in a concrete beam bonded with a soffit plate by including the effect of transverse shear deformation on both the concrete beam and the bonded plate. To accurately predict the distribution of interfacial stresses, Wang (2006) established a bond-slip model to study the interface debonding induced by a flexural crack in an FRP-plated concrete beam. Tounsi and Benyoucef (2007) proposed an analytical method that includes the variation in fiber orientation for an FRP plate to predict the interfacial stress distributions in concrete beams strengthened by composite plates. Recently, Wang and Zhang (2010) presented a three-parameter elastic foundation model for interface stresses in curved beams externally strengthened by a thin FRP plate. Yang and Ye (2010) reported an improved closed-form solution to interfacial stresses in plated beams that uses a two-stage approach. In their solution, beams and bonded plates can be further divided into a number of sub-layers to facilitate the inclusion of steel bars or multiple laminates.

In these existing models, most are limited to a single loading condition in order to obtain a closed-form solution of interface stresses. Few researchers have considered plated beams that are simultaneously subjected to mechanical and thermal loads or mechanical load and prestress. Deng *et al.* (2005), Stratford and Cadei (2006) examined a plated beam under both mechanical and thermal

loading. Klamer *et al.* (2008) reported a comprehensive experimental study on the influence of temperature on strengthened beams. Yang *et al.* (2009) presented an interfacial stress analysis of plated beams under symmetric mechanical and thermal loading. Rabinovitch (2010) analytically investigated the effect of thermal loads on the debonding mechanisms in beams strengthened with externally bonded composite materials by adopting a higher-order stress analysis model and a fracture mechanics mode. Benachour *et al.* (2008) gave a closed-form rigorous solution for interfacial stress in simply supported beams strengthened with bonded prestressed FRP plates.

To uncouple the coupling effect between shear stress and normal stress, a key assumption used in most existing solutions is that the beam and bonded plate have equal curvatures; therefore, the bending moments of the two adherends are proportional to their self-flexural rigidities. Consequently, the contributions of the vertical displacement differences between the two adherends to the adhesive shear deformation and then to the interfacial shear stress are ignored. Based on the deformation compatibility approach developed by Smith and Teng (2001), Hao *et al*. (2010) provided a coupled solution for interfacial stresses by releasing the assumption of equal curvatures when a plated beam is subjected to an external mechanical load and by not considering the effects of adherend shear deformation.

Because accurate predictions of interfacial stresses are a prerequisite for designing structures externally bonded with a plate (Tounsi and Benyoucef 2007), there is a lack of a complete solution that simultaneously considers the effects of the adherend shear deformations, curvature mismatch between the beam and plate, prestress, and mechanical and thermal loads. This study aimed to provide a comprehensive solution for interfacial stresses by incorporating the abovementioned factors. A simply supported beam bonded with a thin prestressing plate and subjected to both mechanical and thermal loading was considered in the present work. The effects of the curvature mismatch and adherend shear deformations of the beam and plate were investigated and compared.

The influence of geometric and material properties on interfacial stresses have attracted a great deal of attention. This paper presents an improved analysis of the main influences on the distribution of interfacial stresses. The interfacial stresses in a plated beam were found to be influenced by the coupled effects of the elastic moduli, which appear as ratios E_a/E_b and E_a/E_p, but not by single changes of them (elastic moduli: adhesive layer (E_a), beam (E_b), and bonded plate (E_p)).

2. Theoretical derivation (Method of solution)

2.1 Interfacial shear stresses: governing differential equation

A differential element of a plated beam, as shown in Fig. 2, can be cut out from the simply supported plated beam shown in Fig. 1, where the interfacial shear and normal stresses are denoted by $\tau(x)$ and $\sigma(x)$, respectively. Fig. 2 also shows the positive sign convention for the bending moment, shear force, axial force, and external applied loading. In this paper, the subscripts b, p, and a denote the beam, plate, and adhesive, respectively.

All materials were assumed to show linear elastic behavior, and the adhesive layer was assumed to be subjected to a constant stress throughout its thickness. The shear strain γ_a in the adhesive layer can be written as

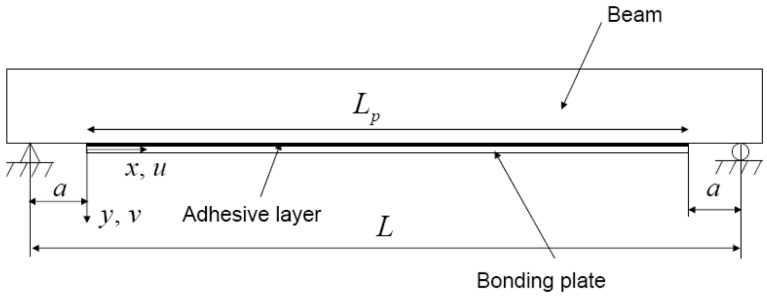

Fig. 1 Simply supported beam bonded with a plate

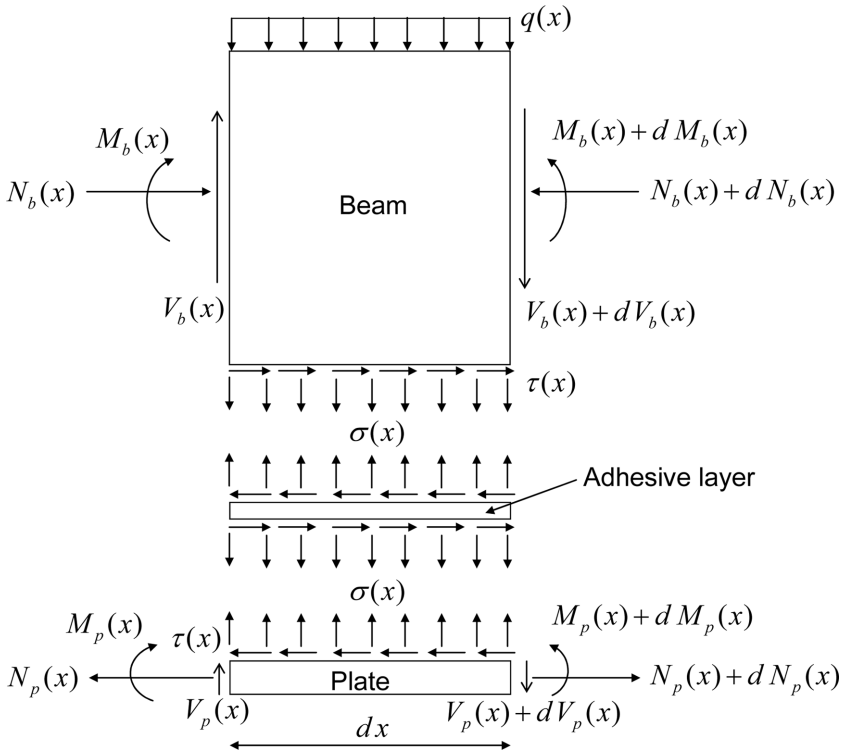

Fig. 2 Differential elements of a plated beam

$$\gamma_a = \frac{\partial u_a(x,y)}{\partial y} + \frac{\partial v_a(x,y)}{\partial x} \tag{1}$$

where $u_a(x,y)$ and $v_a(x,y)$ are the horizontal and vertical displacements, respectively, at any point in the adhesive layer as defined in Fig. 2. The corresponding shear stress is given as

$$\tau(x) = G_a\left(\frac{\partial u_a(x,y)}{\partial y} + \frac{\partial v_a(x,y)}{\partial x}\right) \tag{2}$$

where G_a is the shear modulus of the adhesive layer.

The adhesive was assumed to be subjected to uniform shear stresses; therefore, $u_a(x,y)$ must vary linearly across the adhesive thickness t_a. The

$$\frac{\partial u_a(x,y)}{\partial y} = \frac{1}{t_a}(u_{pa}(x) - u_{ba}(x)) \tag{3}$$

and

$$\frac{\partial^2 u_a(x,y)}{\partial x \partial y} = \frac{1}{t_a}\left(\frac{du_{pa}(x)}{dx} - \frac{du_{ba}(x)}{dx}\right) \tag{4}$$

where u_{pa} and u_{ba} are the longitudinal displacements at the beam-adhesive and plate-adhesive interfaces, respectively.

If the beam is strengthened by being bonded with a prestressed plate, Eq. (4) becomes

$$\frac{\partial^2 u_a(x,y)}{\partial x \partial y} = \frac{1}{t_a}\left(\frac{du_{pa}(x)}{dx} - \frac{P_0}{E_p A_p} - \frac{du_{ba}(x)}{dx}\right) \tag{5}$$

where P_0 is the initial prestressing tension force in the plate; thus, (P_0/E_pA_p) is the longitudinal strain in the plate due to prestressing. E_p is the elastic modulus and A_p, the cross-sectional area of the plate. The prestressing force was assumed to be uniform along the length of plate. The minus sign in $(-P_0/E_pA_p)$ indicates that the initial longitudinal displacement difference between the beam and the plate induced by the prestressing force is opposite to u_{pa}.

In existing solutions, Roberts and Haji-Kazemi (1989), Smith and Teng (2001), Tounsi (2006), and others used $\partial v_a(x,y)/\partial x = 0$ by assuming the beam and plate to have the same curvature. In the present work, mismatch between the curvatures of the beam and plate was considered

$$\frac{\partial v_a^2(x,y)}{\partial x^2} = \frac{1}{2}\left(\frac{dv_p^2(x)}{dx^2} + \frac{dv_b^2(x)}{dx^2}\right) \tag{6}$$

where $v_p(x)$ and $v_b(x)$ are the vertical displacements of the plate and beam, respectively. Because linear elastic behavior was assumed for all materials and the adhesive layer is very thin, the stresses can be assumed to be constant throughout the layer thickness. Therefore, $u(x,y)$ varies linearly across the adhesive thickness in every differential element. Thus, when deriving Eq. (6), assuming that the curvature of the mid-plane of the adhesive layer is the average of the curvatures of the beam and bonded plate is acceptable.

Differentiating Eq. (2) with respect to x and using (5) and (6) gives

$$\frac{d\tau(x)}{dx} = \frac{G_a}{t_a}\left(\left(\frac{du_{pa}(x)}{dx} - \frac{P_0}{E_p A_p} - \frac{du_{ba}(x)}{dx}\right) + \frac{t_a}{2}\left(\frac{d^2 v_p(x)}{dx^2} + \frac{d^2 v_b(x)}{dx^2}\right)\right) \tag{7}$$

The longitudinal shear deformations of both the beam and the plate are incorporated here. It is reasonable to assume that the shear stresses that develop in the adhesive are continuous across the adhesive-adherend interface. In addition, equilibrium requires the shear stress be zero at the free surface. Using the same methodology developed by Tsai *et al.* (1998) and Tounsi *et al.* (2009), a parabolic variation of the longitudinal displacements $U_b^N(x,y_b')$ and $U_p^N(x,y_p')$ in the beam and plate was assumed, i.e.

$$U_b^N = A_b(x){y_b'}^3 + B_b(x)y_b' + C_b(x) \tag{8}$$

$$U_p^N = A_p(x)y_p'^3 + B_p(x)y_p' + C_p(x) \tag{9}$$

y_b' (or y_p') is a local coordinate system with the origin at the top surface of the beam (or plate).
The shear strains in the beam (plate) are

$$\gamma_b = \frac{\partial u_b^N}{\partial y_b'} + \frac{\partial w_b^N}{\partial y_b'} \tag{10}$$

$$\gamma_p = \frac{\partial u_p^N}{\partial y_p'} + \frac{\partial w_p^N}{\partial y_p'} \tag{11}$$

Neglecting the variations in transverse displacements W_b^N and W_p^N induced by the longitudinal forces with the longitudinal coordinate x

$$\gamma_b \approx \frac{\partial u_b^N}{\partial y_b'} \tag{12}$$

$$\gamma_p \approx \frac{\partial u_p^N}{\partial y_p'} \tag{13}$$

Thus, the shear stresses in the beam (plate) are

$$\tau_b = G_b(3A_b(x)y_b'^2 + B_b(x)) \tag{14}$$

$$\tau_p = G_p(3A_p(x)y_p'^2 + B_p(x)) \tag{15}$$

The continuity condition and the assumption of uniform shear stresses throughout the thickness of adhesive gives $\tau(x) = \tau_a$ and

$$\tau_b(x, h_b) = \tau_p(x, 0) = \tau(x) = \tau_a \tag{16}$$

There is no shear stress at the top surface of the beam (at $y_b' = 0$) and the bottom surface of the plate (at $y_p' = h_p$); then

$$\tau_b(x, 0) = 0\,, \quad \tau_p(x, h_p) = 0 \tag{17}$$

where h_b and h_p are the thicknesses of the beam and plate, respectively.
Substituting Eqs. (14) and (15) into Eqs. (16) and (17) yields

$$\tau_b = \frac{y_b'^2}{h_b^2}\tau(x) \tag{18}$$

$$\tau_p = \left(1 - \frac{y_p'^2}{h_p^2}\right)\tau(x) \tag{19}$$

The corresponding shear strains are

$$\gamma_b = \frac{y_b'^2}{h_b^2}\frac{\tau(x)}{G_b} \tag{20}$$

and

$$\gamma_p = \left(1 - \frac{y_p'^2}{h_p^2}\right)\frac{\tau(x)}{G_p} \tag{21}$$

The longitudinal displacement functions u_b^N for the beam and u_p^N for plate, due to the longitudinal forces, are given as

$$u_b^N(y_b) = u_{ba}^N + \int_{h_b}^{y_b}\gamma_b(y_b')dy_b' = u_{ba}^N + \frac{\tau(x)}{3G_b h_b^2}y_b'^3 - \frac{\tau(x)}{3G_b}h_b \tag{22}$$

$$u_p^N(y_p) = u_{pa}^N + \int_0^{y_p}\gamma_p(y_p')dy_p' = u_{pa}^N + \frac{\tau(x)}{G_p}\left(y_p' - \frac{y_p'^3}{3h_p^2}\right) \tag{23}$$

where u_{ba}^N and u_{pa}^N represent the displacement at the interface between the adhesive and the beam or plate, respectively, due to the longitudinal forces.

The longitudinal resultant forces N_b and N_p for the rectangular beam and plate are

$$N_b = E_b b_p \int_0^{h_b}\frac{du_b^N}{dx}dy_b' = E_b A_b\left(\frac{du_{ba}^N}{dx} - \frac{h_b}{4G_b}\frac{d\tau}{dx}\right) \tag{24}$$

and

$$N_p = E_p b_p \int_0^{h_p}\frac{du_p^N}{dx}dy_p' = E_p A_p\left(\frac{du_{pa}^N}{dx} + \frac{5h_p}{12G_p}\frac{d\tau}{dx}\right) \tag{25}$$

The resultant deformation of the interface between the beam (or plate) and the adhesive combines the deformations induced by both the longitudinal force and the bending moment at the beam (plate); they can be expressed as

$$u_{ba} = u_{ba}^N + u_{ba}^M \tag{26}$$

and

$$u_{pa} = u_{pa}^N + u_{pa}^M \tag{27}$$

The strains are then

$$\varepsilon_{pa} = \frac{du_{pa}}{dx} = -\frac{y_p}{E_p I_p}M_p(x) + \frac{1}{E_p A_p}N_p(x) - \frac{5h_p}{12G_p}\frac{d\tau(x)}{dx} \tag{28}$$

for the interface between the plate and adhesive and

$$\varepsilon_{ba} = \frac{du_{ba}}{dx} = \frac{y_b}{E_b I_b}M_b(x) - \frac{1}{E_b A_b}N_b(x) + \frac{h_b}{4G_b}\frac{d\tau(x)}{dx} \tag{29}$$

for the interface between the beam and adhesive.

E_b is the elastic modulus of the beam and A_b, the cross-sectional area of the beam. I_b and I_p are the second moments of area. M_b (or M_p) is the bending moment and N_b (or N_p), the axial force. y_b and y_p are the distances from the bottom of the beam and the top of the plate to their respective centroids, respectively.

When the thermal load is also considered, Eqs. (28) and (29) can be rewritten as

$$\varepsilon_{pa} = \frac{du_{pa}}{dx} = -\frac{y_p}{E_p I_p} M_p(x) + \frac{1}{E_p A_p} N_p(x) - \frac{5h_p}{12G_p} \frac{d\tau(x)}{dx} + \alpha_p \Delta T \tag{30}$$

and

$$\varepsilon_{ba} = \frac{du_{ba}}{dx} = \frac{y_b}{E_b I_b} M_b(x) - \frac{1}{E_b A_b} N_b(x) + \frac{h_b}{4G_b} \frac{d\tau(x)}{dx} + \alpha_b \Delta T \tag{31}$$

α_b and α_p are the thermal expansion coefficients of the beam and plate, respectively. ΔT is the temperature elevation.

The transverse shear deformations in both the beam and the bonded plate are ignored here; the equilibrium of the plate and beam then gives the following relationships.

For the plate

$$\frac{d^2 v_p(x)}{dx^2} = -\frac{1}{E_p I_p} M_p(x) \tag{32}$$

$$\frac{dM_p(x)}{dx} = V_p(x) - b_p y_p \tau(x) \tag{33}$$

$$\frac{dV_p(x)}{dx} = b_p \sigma(x) \tag{34}$$

For the beam

$$\frac{d^2 v_b(x)}{dx^2} = -\frac{1}{E_b I_b} M_b(x) \tag{35}$$

$$\frac{dM_b(x)}{dx} = V_b(x) - b_p y_b \tau(x) \tag{36}$$

$$\frac{dV_b(x)}{dx} = -b_p \sigma(x) - q \tag{37}$$

The horizontal equilibrium gives

$$\frac{dN_p(x)}{dx} = \frac{dN_b(x)}{dx} = b_p \tau(x) \tag{38}$$

$$\frac{d^2 N_p(x)}{dx^2} = \frac{d^2 N_b(x)}{dx^2} = b_p \frac{d\tau(x)}{dx} \tag{39}$$

where b_p is the width of the plate. The beam and plate were assumed to have the same width.

Substituting the above equations into Eq. (7), we obtain

$$\frac{d\tau(x)}{dx} = \frac{G_a}{t_a}\left[\left(-\frac{y_p}{E_pI_p}M_p(x) + \frac{1}{E_pA_p}N_p(x) - \frac{h_p}{3G_p}\frac{d\tau(x)}{dx} + \alpha_p\Delta T - \frac{y_b}{E_bI_b}M_b(x) - \frac{P_0}{E_pA_p}\right.\right.$$

$$\left.\left. + \frac{1}{E_bA_b}N_b(x) - \frac{h_b}{3G_b}\frac{d\tau(x)}{dx} + \alpha_b\Delta T\right) + \frac{t_a}{2}\left(-\frac{1}{E_pI_p}M_p(x) - \frac{1}{E_bI_b}M_b(x)\right)\right] \tag{40}$$

Differentiating Eq. (40) with respect to x twice gives

$$\frac{d^3\tau(x)}{dx^2} = \frac{G_a}{t_a}\left(\left(\frac{d^3u_{pa}(x)}{dx^3} - \frac{d^3u_{ba}(x)}{dx^3}\right) + \frac{t_a}{2}\left(\frac{d^4v_p(x)}{dx^4} + \frac{d^4v_b(x)}{dx^4}\right)\right) \tag{41}$$

Based on the above equilibrium equations, the fourth derivative of the vertical displacement can be written as

$$\frac{d^4v_p(x)}{dx^4} = -\frac{1}{E_pI_p}\left(b_p\sigma(x) - b_py_p\frac{d\tau(x)}{dx}\right) \tag{42}$$

$$\frac{d^4v_b(x)}{dx^4} = \frac{1}{E_bI_b}\left(b_p\sigma(x) + q + b_py_b\frac{d\tau(x)}{dx}\right) \tag{43}$$

and the third derivative of the horizontal displacement can be written as

$$\frac{d^3u_{pa}(x)}{dx^3} = -\frac{y_p}{E_pI_p}\left(b_p\sigma(x) - b_py_p\frac{d\tau(x)}{dx}\right) + \frac{1}{E_pA_p}b_p\frac{d\tau(x)}{dx} - \frac{5h_p}{12G_p}\frac{d^3\tau(x)}{dx^3} \tag{44}$$

$$\frac{d^3u_{ba}(x)}{dx^3} = -\frac{y_b}{E_bI_b}\left(b_p\sigma(x) + q + b_py_b\frac{d\tau(x)}{dx}\right) - \frac{1}{E_bA_b}b_p\frac{d\tau(x)}{dx} + \frac{h_b}{4G_b}\frac{d^3\tau(x)}{dx^3} \tag{45}$$

By substituting Eqs. (42)-(45) into Eq. (41), the governing differential equation for the interfacial shear stresses can be written as

$$\alpha_0\frac{d^3\tau(x)}{dx^3} = \alpha_1\frac{d\tau(x)}{dx} + \alpha_2\sigma(x) + \alpha_3 q \tag{46}$$

where $\alpha_0 = 1 + \frac{G_a}{t_a}\frac{5h_p}{12G_p} + \frac{G_a}{t_a}\frac{h_b}{4G_b}$

$$\alpha_1 = \frac{G_a}{t_a}\left(\frac{b_py_p^2}{E_pI_p} + \frac{b_p}{E_pA_p} + \frac{b_py_b^2}{E_bI_b} + \frac{b_p}{E_bA_b} + \frac{t_a}{2}\frac{b_py_p}{E_pI_p} + \frac{t_a}{2}\frac{b_py_b}{E_bI_b}\right)$$

$$\alpha_2 = \frac{G_a}{t_a}\left(\frac{y_b}{E_bI_b} - \frac{y_p}{E_pI_p} + \frac{t_a}{2}\frac{1}{E_bI_b} - \frac{t_a}{2}\frac{1}{E_pI_p}\right)b_p, \quad \alpha_3 = \frac{G_a}{t_a}\left(\frac{y_b}{E_bI_b} + \frac{t_a}{2}\frac{1}{E_bI_b}\right)$$

2.2 Interfacial normal stresses: governing differential equation

When the beam is loaded, vertical separation occurs between the beam and the plate. This separation leads to different curvatures of the beam and plate and creates an interfacial normal stress

in the adhesive layer. The normal stress $\sigma(x)$ is given as

$$\sigma(x) = \frac{E_a}{t_a}(v_p(x) - v_b(x)) \tag{47}$$

Substituting Eqs. (42) and (43) into the fourth derivative of the interfacial normal stress obtained from Eq. (47) gives the following governing differential equation for the interfacial normal stress

$$\frac{d^4\sigma(x)}{dx^4} + \beta_1\sigma(x) + \beta_2\frac{d\tau(x)}{dx} + \beta_3 q = 0 \tag{48}$$

where $\beta_1 = \frac{E_a b_p}{t_a}\left(\frac{1}{E_b I_b} + \frac{1}{E_p I_p}\right)$, $\beta_2 = \frac{E_a b_p}{t_a}\left(\frac{y_b}{E_b I_b} - \frac{y_p}{E_p I_p}\right)$, $\beta_3 = \frac{E_a}{t_a}\frac{1}{E_b I_b}$.

3. General solutions for the interfacial shear and normal stresses

The governing differential equations for the interfacial shear and normal stresses (Eqs. (46) and (48)) are clearly coupled; the task becomes to seek the solution of the following differential equation system

$$\begin{cases} \alpha_0\frac{d^3\tau(x)}{dx^3} = \alpha_1\frac{d\tau(x)}{dx} + \alpha_2\sigma(x) + \alpha_3 q \\ \frac{d^4\sigma(x)}{dx^4} + \beta_1\sigma(x) + \beta_2\frac{d\tau(x)}{dx} + \beta_3 q = 0 \end{cases} \tag{49}$$

For simplicity, the general solutions presented below are limited to loading that is either concentrated or uniformly distributed over part of the span of the beam, the whole span, or both. For such loadings, the second and higher-order derivatives of the load are zero.

Let $D = d/dx^2$; then, the above expressions can be written as

$$\begin{cases} (\alpha_0 D^3 - \alpha_1 D)\tau = \alpha_2\sigma(x) + \alpha_3 q \\ (D^4 + \beta_1)\sigma + \beta_2 D\tau + \beta_3 q = 0 \end{cases} \tag{50}$$

The first equation of (50) gives

$$\sigma = \frac{(\alpha_0 D^3 - \alpha_1 D)\tau(x) - \alpha_3 q}{\alpha_2} \tag{51}$$

Substituting (51) into the second Equation of (50) gives

$$(\alpha_0 D^7 + \alpha_0\beta_1 D^3 - \alpha_1 D^5 - \alpha_1\beta_1 D)\tau + \alpha_2\beta_2 D\tau + \alpha_2\beta_3 q - \alpha_3 D^4 q - \alpha_3\beta_1 q = 0 \tag{52}$$

By assuming $d^5\tau/dx^5 = 0$ because $d^5\tau/dx^5$ is generally negligible to the final solution (Smith and Teng 2001), the general solution of interfacial shear stresses can be easily given by

$$\tau(x) = C_1 + C_2 e^{\sqrt{m}x} + C_3 e^{-\sqrt{m}x} + nqx \tag{53}$$

where $m = \dfrac{\alpha_1\beta_1 - \alpha_2\beta_2}{\alpha_0\beta_1}$ and $n = \dfrac{\alpha_3\beta_1 - \alpha_2\beta_3}{\alpha_2\beta_2 - \alpha_1\beta_1}$. It is not difficult to find $m > 0$.

Substituting (53) into the second equation of (50) gives

$$D^4\sigma + \beta_1\sigma = -C_1\beta_2\sqrt{m}e^{\sqrt{m}x} + C_2\beta_2\sqrt{m}e^{-\sqrt{m}x} - (n\beta_2 + \beta_3)q \tag{54}$$

The solution of this equation can be written as

$$\sigma(x) = e^{kx}(B_1\cos kx + B_2\sin kx) + e^{-kx}(B_3\cos kx + B_4\sin kx) + \sigma^*(x) \tag{55}$$

where $k = \sqrt[4]{\beta_1/4}$ and $\sigma^*(x)$ is the particular solution.

Assuming the particular solution

$$\sigma^*(x) = C_1 e^{\sqrt{m}x} + C_2 e^{-\sqrt{m}x} + G_3 \tag{56}$$

and substituting it into (53) gives $G_1 = \dfrac{-\beta_2 C_1\sqrt{m}}{m^2 + \beta_1}$, $G_2 = \dfrac{\beta_2 C_2\sqrt{m}}{m^2 + \beta_1}$, and $G_3 = -\dfrac{\beta_2 n + \beta_3}{\beta_1}q$.

Then, the general solution for normal stress is

$$\begin{aligned}\sigma(x) = {} & e^{kx}(B_1\cos kx + B_2\sin kx) + e^{-kx}(B_3\cos kx + B_4\sin kx) \\ & + \frac{\beta_2 C_3\sqrt{m}}{m^2 + \beta_1}e^{-\sqrt{m}x} - \frac{\beta_2 C_2\sqrt{m}}{m^2 + \beta_1}e^{\sqrt{m}x} - \frac{(\beta_2 n + \beta_3)q}{\beta_1}\end{aligned} \tag{57}$$

Because $\beta_2 < 0$ and the normal stress tends to be zero when x is very large, the coefficients $C_2 = B_1 = B_2 = 0$ and the normal stress can be expressed as

$$\sigma(x) = e^{-kx}(B_3\cos kx + B_4\sin kx) + \frac{\beta_2 C_3\sqrt{m}}{m^2 + \beta_1}e^{-\sqrt{m}x} - \frac{(\beta_2 n + \beta_3)q}{\beta_1} \tag{58}$$

4. Interfacial stresses for a uniformly distributed load

We now compare the results predicted by the present method with others through an example where the plated beam is subjected to an uniformly distributed load q. The first step is to determine the parameters B_3, B_4 and C_1, C_3 in Eqs. (53) and (58) from the boundary conditions:

1) The first boundary condition requires zero interfacial shear stress at the mid-span due to symmetry of the applied load: i.e., $\tau(L_p/2) = 0$ when $x = L_p/2$. Substituting these into Eq. (53) gives

$$nq\left(\frac{L_p}{2}\right) + C_1 + C_3 e^{-\sqrt{m}\left(\frac{L_p}{2}\right)} = 0 \tag{59}$$

$e^{-\frac{L_p}{2}\sqrt{m}}$ tends to zero when L_p is very large, so $C_1 = -n\frac{L_p}{2}q$.

2) The second boundary condition is the applied bending moment at $x = 0$. Here, the moment $M_p(0)$ at the plate end and the axial resultant force of either the beam or plate $N_b(0) = N_p(0)$ are zero: i.e., $M_p(0) = 0$ and $N_b(0) = N_p(0)$.

Subsequently, the moment in the section at the end of plate is resisted by only the beam; we can then obtain $M_b(0) = M_T(0) = \frac{qa}{2}(L-a)$. From Eq. (40), we can obtain

$$\left.\frac{d\tau}{dx}\right|_{x=0} = \left[-\left(y_b + \frac{t_a}{2}\right)\frac{M_b(0)}{E_bI_b} + (\alpha_p - \alpha_b)\Delta T - \frac{P_0}{E_pA_p}\right]\frac{G_a}{t_a\alpha_0} \tag{60}$$

From Eq. (53)

$$\left.\frac{d\tau}{dx}\right|_{x=0} = nq - C_3\sqrt{m} \tag{61}$$

Substituting Eq. (60) into (61) gives

$$C_3 = \frac{nq + \frac{G_a}{t_a\alpha_0}\left[\left(y_b + \frac{t_a}{2}\right)\frac{M_b(0)}{E_bI_b} - (\alpha_p - \alpha_b)\Delta T + \frac{P_0}{E_pA_p}\right]}{\sqrt{m}}$$

On the other hand, Eq. (58) gives

$$\left.\frac{d^2\sigma(x)}{dx^2}\right|_{x=0} = -2k^2B_4 + \frac{\beta_2C_3m^{3/2}}{m^2 + \beta_1} \tag{62}$$

From Eq. (47), we obtain

$$\frac{d^2\sigma(x)}{dx^2} = \frac{E_a}{t_a}\left(\frac{d^2v_p(x)}{dx_2} - \frac{d^2v_b(x)}{dx^2}\right) \tag{63}$$

Substituting Eqs. (32) and (35) into Eq. (63) gives

$$\frac{d^2\sigma(x)}{dx^2} = \frac{E_a}{t_a}\left(-\frac{1}{E_pI_p}M_p(x) + \frac{1}{E_bI_b}M_b(x)\right) \tag{64}$$

Substituting the boundary conditions $M_p(0) = 0$, $M_b(0) = qa(L-a)/2$ into Eq. (64) gives

$$\left.\frac{d^2\sigma(x)}{dx^2}\right|_{x=0} = \frac{E_aqa(L-a)}{2t_aE_bI_b} \tag{65}$$

By combining Eqs. (62) and (65), we obtain

$$B_4 = \frac{\beta_2C_3m^{3/2}}{2(m^2 + \beta_1)k^2} - \frac{E_aqa(L-a)}{4t_aE_bI_bk^2} \tag{66}$$

3) The resultant shear force at the end of the plate is zero: i.e., $V_p(0) = 0$, $V_p(0) = V_T(0)$, and $V_T(0) = ql/2 - qa$. From Eq. (47), we can obtain

$$\frac{d^3\sigma(x)}{dx^3} = \frac{E_a}{t_a}\left(\frac{d^3v_p(x)}{dx^3} - \frac{d^3v_b(x)}{dx^3}\right) \tag{67}$$

Substituting Eqs. (32), (33), (35), and (36) into Eq. (67) gives

$$\frac{d^3\sigma(x)}{dx^3} = \frac{E_a}{t_a}\left[-\frac{1}{E_pI_p}(V_p(x) - b_py_p\tau(x)) + \frac{1}{E_bI_b}(V_b(x) - b_py_b\tau(x))\right] \tag{68}$$

Substituting boundary conditions $V_p(0) = 0$ and $V_p(0) = V_T(0)$ into Eq. (68) gives

$$\left.\frac{d^3\sigma(x)}{dx^3}\right|_{x=0} = \beta_3V_T(0) - \beta_2\tau(0) \tag{69}$$

From Eq. (58), we can obtain

$$\left.\frac{d^3\sigma(x)}{dx^3}\right|_{x=0} = 2k^3B_3 + 2k^3B_4 - \frac{\beta_2C_3m^2}{m^2+\beta_1} \tag{70}$$

Combining Eqs. (69) and (70) gives

$$B_3 = \frac{\beta_3V_T(0) - \beta_2\tau(0) + \dfrac{\beta_2C_3m^2}{m^2+\beta_1} - 2k^3B_4}{2k^3} \tag{71}$$

5. Results

To verify the analytical model, the present predictions were first compared with those of Tousi (2006), Tousi *et al.* (2009), Hao *et al.* (2010), and Smith and Teng (2001), both the prestressing force and thermal loads were ignored. The effects of curvature mismatch and adherend shear deformation were then considered when the plated beam was subjected to mechanical loads, prestressing, and thermal loads. Finally, the effects of various parameters on the distributions of the interfacial stresses were investigated.

5.1 Main parameters influencing the distribution of interfacial stresses

The parameters that affect the distribution of interfacial stresses have been investigated by many researchers. The interfacial shear and normal stresses can expressed as

$$\sigma(\text{or } \tau) = f(h_b, b_b, L; L_p, h_p, b_p; t_a; E_b, E_p, E_a, \mu_b, \mu_p, \mu_a; q, P_0, \Delta T) \tag{72}$$

The strengthened beam is already *in situ*; thus, the mechanical properties (E_b and μ_b) and the sizes (h_b, b_b, L) of the beam are also fixed. q is the external load on the beam, and the width b_p of the plate is generally equal to that of the beam b_b. Thus, the main parameters that influence the distribution of interfacial stresses include $L_p, h_p; t_a; E_b, E_p, E_a, \mu_b, \mu_p, \mu_a; P_0, \Delta T$. From the above derivation, E_b, E_p, E_a are usually coupled as E_a/E_b and E_a/E_p. Consequently, we focused on the effects of P_0, ΔT, E_a/E_b, E_a/E_p, h_p, L_p, and t_a on the interfacial stresses. In addition, future

Table 1 Geometric and material properties

Component	Width(mm)	Depth(mm)	Young's Modulus (MPa)	Poisson's ratio
RC beam	200	300	30000	0.2
CFRP plate	200	4	100,000	0.3
Adhesive layer	200	2	2000	0.35

research will examine the impact of temperature on interfacial stresses by incorporating the temperature-dependent elastic and shear moduli of the adhesive.

5.2 Geometric and material properties

An RC beam bonded with CFRP plate was analyzed. Table 1 summarizes the geometric and material properties. The beam was simply supported and subjected to a uniformly distributed load (UDL) q = 50 N/mm. The span of the beam was L = 3000 mm; the distance from the support to the end of the plate was a = 300 mm.

5.3 Comparison with other solutions when $P_0 = 0$ and $\Delta T = 0$

To compare the results obtained with the present theory and the existing solutions, first consider a plated beam carrying only mechanical loads but neither prestress nor thermal loads. The effects of both curvature mismatch and adherend shear deformation should both be demonstrated to be considered in the present analyses. Tousi (2006) and Tousi *et al.* (2009) produced results that included the effect of adherend shear deformation but did not include the effect of curvature mismatch. Hao *et al*. (2010) considered the effect of curvature mismatch but did not consider the effect of adherend shear deformation. Neither of these effects were considered in Smith and Teng's (2001) solution.

Figs. 3(a) and (b) plot the distributions of interfacial shear and normal stresses, respectively, near the plate end for an RC beam bonded with a CFRP plate as calculated by these four methods. The

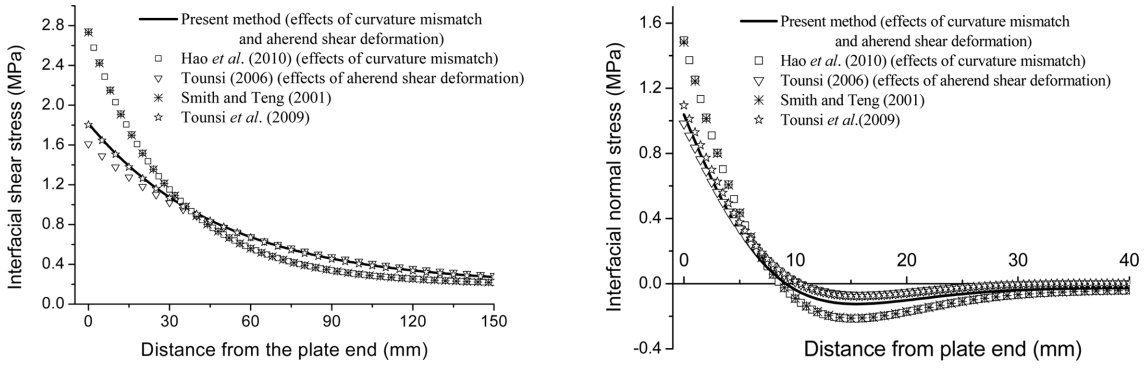

(a) (b)

Fig. 3 Comparison of interfacial shear and normal stresses for a plated beam subjected to a UDL. (a) shear stress, (b) normal stress

Table 2 Comparison of peak interfacial shear and normal stresses

	Present method	Tousi (2006)	Hao *et al.* (2010)	Smith and Teng (2001)	Tousi *et al*. (2009)
τ_{max} (MPa)	1.817	1.612	2.760	2.740	1.803
σ_{max} (MPa)	1.038	0.982	1.495	1.484	1.094

solutions from this work, Tousi (2006), and Tousi *et al.* (2009) gave lower maximum interfacial shear and normal stresses than those predicted by Smith and Teng (2001) and Hao *et al.* (2010). However, the differences between the present results and those of Tousi *et al.* (2009) and the discrepancy in the solutions of Smith and Teng (2001) and Hao *et al.* (2010) were both small. This indicates that the inclusion of adherend shear deformation leads to lower values of τ_{max} and σ_{max} and thus reduces the level of stress concentration. However, the influence of curvature mismatch on interfacial stresses is small, even though it may induce larger interfacial stresses (Table 2). The maximum interfacial shear and normal stresses given by Tousi (2006) may be lower than the results of this work and those of Tousi *et al.* (2009) because the assumptions used in the theories of this work and by Tousi *et al.* (2009) agree with the beam theory (parabolic distribution of shear stresses through the depth of the beam).

5.4 Effects of curvature mismatch and adherend shear deformation when $P_0 \neq 0$ and $\Delta T \neq 0$

Fig. 4 shows the results for a beam strengthened by a prestressed CFRP plate. The prestressing force $P_0 = 100$ kN and temperature elevation $\Delta T = 20^oC$. The coefficients of thermal expansion were 1.2×10^{-5} $^oC^{-1}$ for the concrete and 0.2×10^{-5} $^oC^{-1}$ for the CFRP plate, but the variation in elastic modulus with temperature was not considered here. The effects of both curvature mismatch and adherend shear deformation presented a similar tendency to the case discussed in section 5.2 when $P_0 = 0$ and $\Delta T = 0$. Consequently, prestressing and thermal loads do not change the contribution of

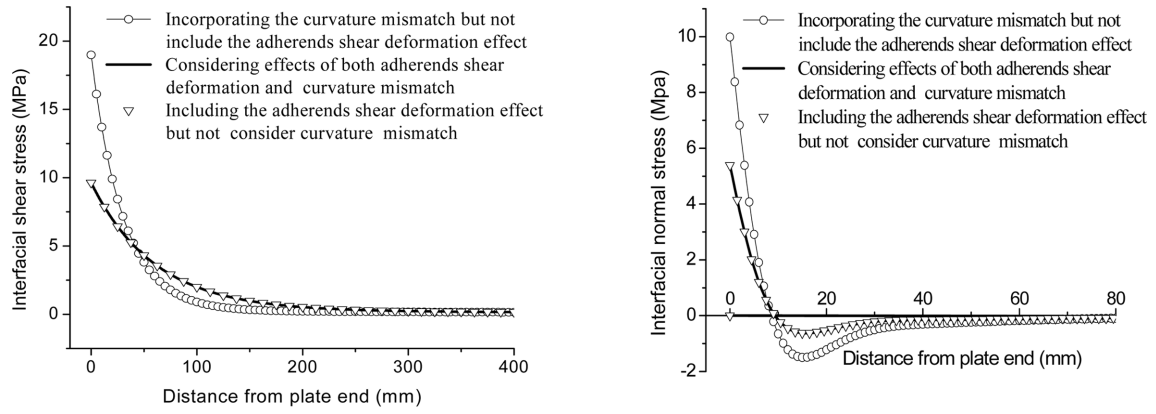

(a) (b)

Fig. 4 Effects of curvature mismatch and adherends shear deformation on interfacial stresses. (a) shear stress, (b) normal stress

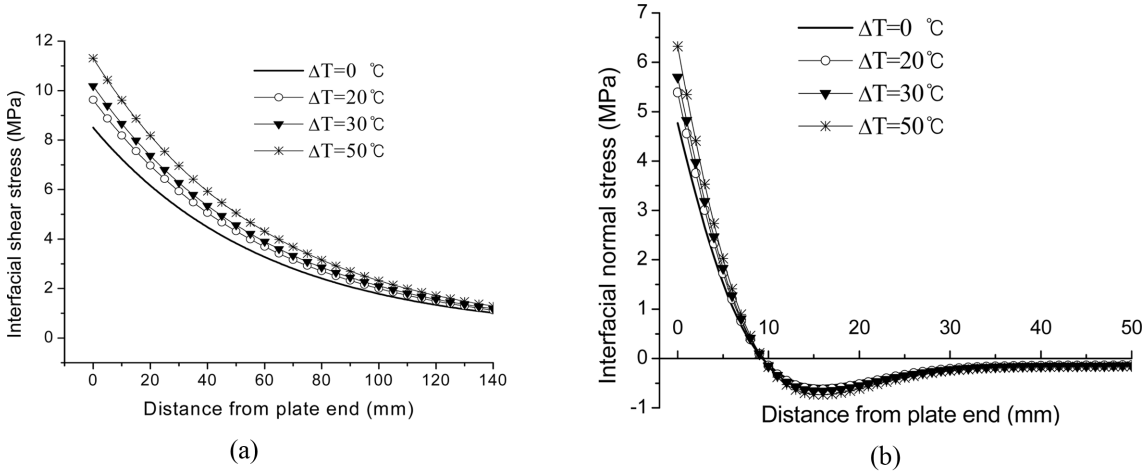

Fig. 5 Effects of temperature elevation (ΔT) on interfacial stresses. (a) shear stress, (b) normal stress

either adherend shear deformation or curvature mismatch to the interfacial stresses. The inclusion of the adherend shear deformation effect on the beam and plate remarkably reduces the values of the maximum interfacial shear and normal stresses.

5.5 Effects of temperature elevation (ΔT)

As the beam and plate material (e.g., concrete, steel, and FRP) generally have different thermal expansion coefficients, large thermal stresses may arise in the plated beam because of temperature changes (either increases or decreases). The effect of the difference in thermal expansion of two adherends on the interfacial stresses was considered for four cases: ΔT = 0, 20, 30, and 50°C. The variation in mechanical properties such as the elastic modulus of the adhesive was not considered. For the initial prestressing force, $P_0 = 100$ kN. Fig. 5 shows that an increase in temperature elevation (ΔT) results in a higher stress concentration and higher interfacial shear and normal stresses.

5.6 Effects of the prestressing force (P_0) on interfacial stresses

The edge interfacial shear and normal stresses of a plated beam with variable prestressing force were compared. Four cases of constant prestressing forces were examined: P_0 = 0, 60, 100, and 120 kN. A uniformly distributed external load of q = 50 N/mm was assumed. As shown in Fig. 6, an increase in the initial prestressing force (P_0) clearly leads to a high stress concentration.

5.7 Parametric study

To better understand the behavior of the plated beam, the influence of various parameters on the values of interfacial stresses were investigated. A case of a plated beam strengthened by a bonded prestressing plate subjected to both mechanical and thermal loads was considered; the presented solutions include both the effects of curvature mismatch and adherend deformation. The initial

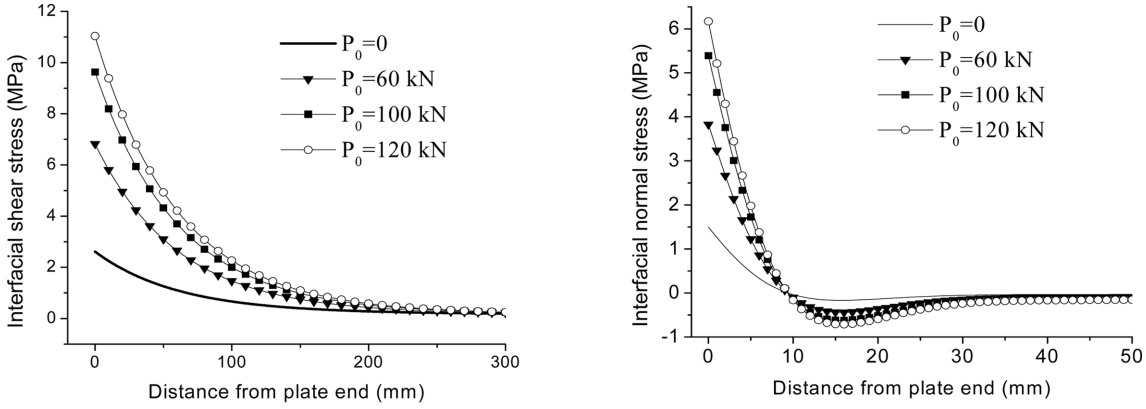

(a) (b)

Fig. 6 The effect of the prestressing force (P_0) on interfacial stresses. (a) shear stress, (b) normal stress

prestressing force was set to P_0 = 100 kN, and the uniformly distributed external load was q = 50 N/mm.

5.7.1 Effects of the ratios E_a/E_b and E_a/E_p

Many researchers have investigated the respective effects of the elastic moduli of the adhesive layer (E_a), beam (E_b), and bonded plate (E_p). However, Eqs. (49), (53), and (58) make it clear that these three parameters are coupled and appear as ratios E_a/E_b and E_a/E_p. From the analytical solutions of the interfacial stresses (see Eqs. (53) and (58)), the interfacial stresses do not change if both E_a/E_b and E_a/E_p are kept constant when the thermal effect is not considered.

Fig. 7 shows the interfacial shear and normal stresses when E_a/E_b is equal to 1/30, 3/30, and 6/30 but E_a/E_p is kept constant as 1/100. The results when E_a/E_b was kept constant at 1/10 and E_a/E_p was 1/100, 3/100, and 6/100, are shown in Fig. 8. The modulus ratios clearly affected both the

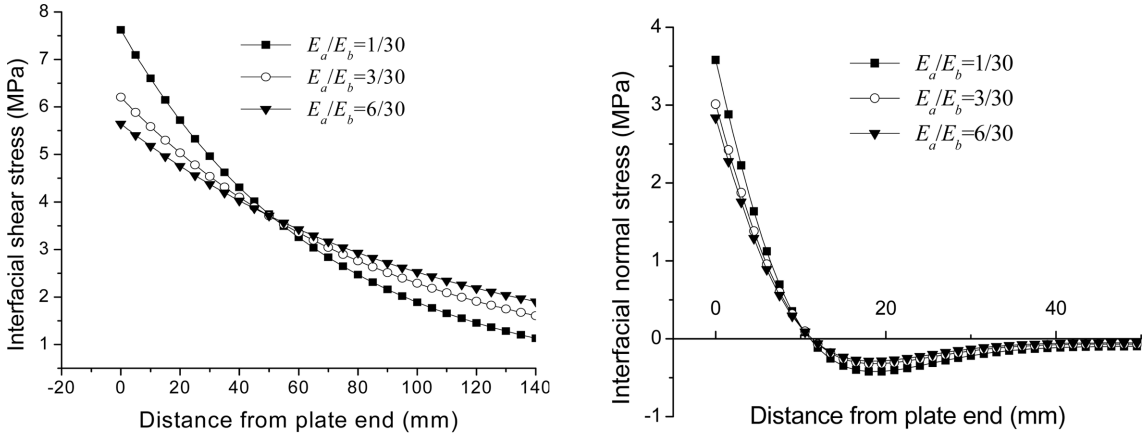

(a) (b)

Fig. 7 Effects of the ratio E_a/E_b when E_a/E_p is kept as 1/100. (a) shear stress, (b) normal stress

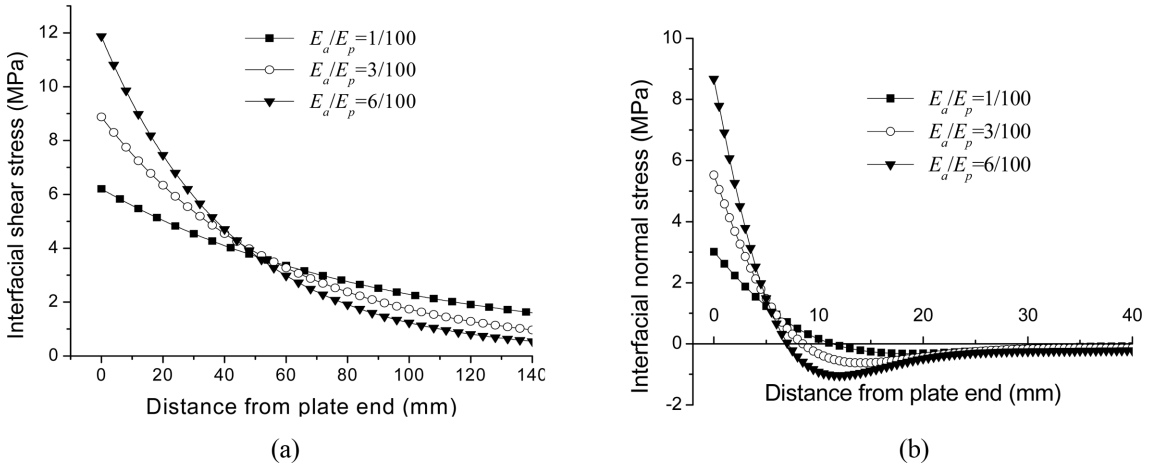

Fig. 8 Effects of the ratio E_a/E_p when E_a/E_b is kept as 1/10. (a) shear stress, (b) normal stress

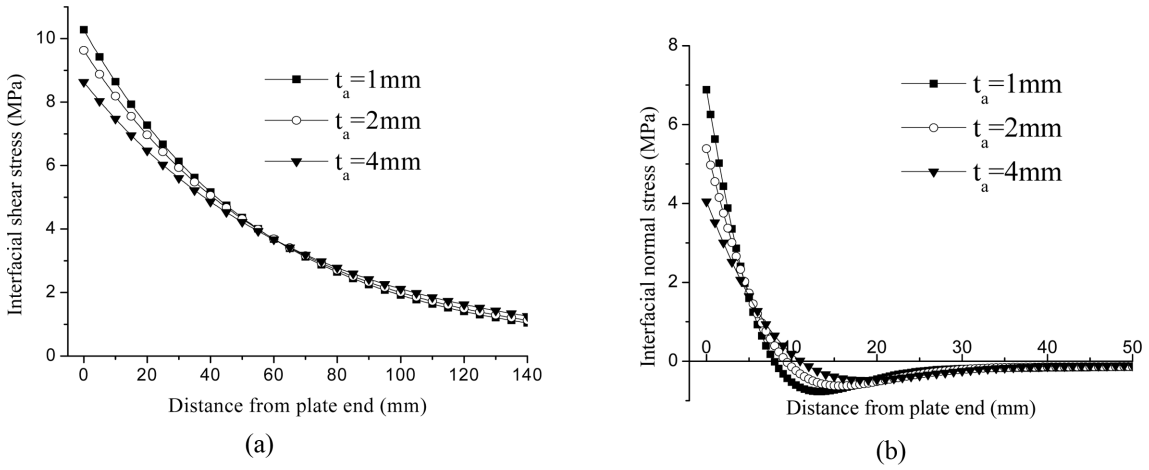

Fig. 9 Effects of thickness of the adhesive layer on interfacial stresses. (a) shear stress, (b) normal stress

interfacial shear and the normal stresses to a substantial degree. Increasing E_a/E_b produced lower interfacial stress values, but increasing E_a/E_p increased the interfacial stresses.

5.7.2 Effects of adhesive layer thickness

The thickness of the adhesive layer is a significant parameter. Fig. 9 shows the effect of the adhesive layer thickness on interfacial stresses. The level of stress concentration decreased with increased thickness of the adhesive layer.

5.7.3 Effects of plate thickness and length

The thickness of the bonded plate is an important design variable in practice (Tousi *et al.* 2009). Fig. 10 shows the effect of the thickness of the plate on the interfacial stresses. Three thicknesses of h_p = 1, 2, and 4 mm were considered for a constant length L_p = 2400 mm. The interfacial stresses

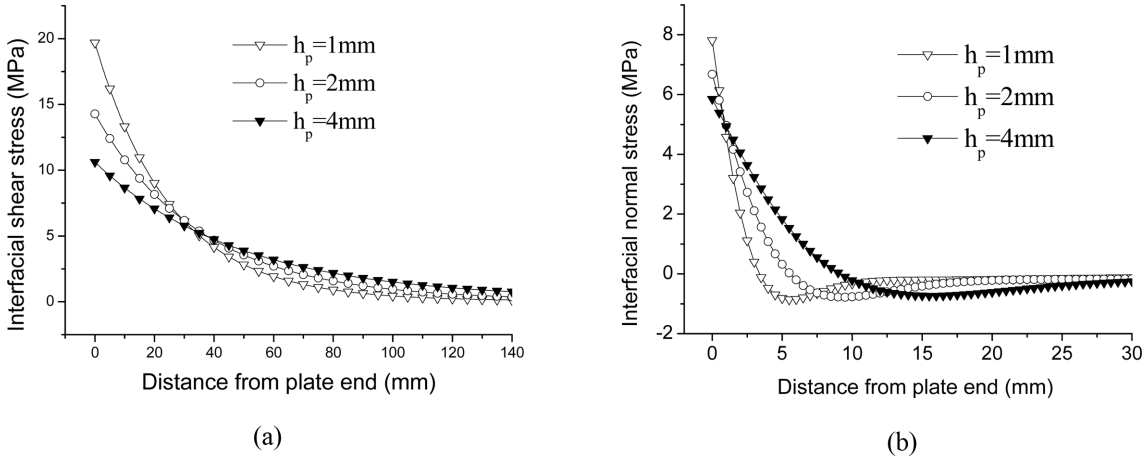

Fig. 10 The effect of plate thickness on interfacial stresses when $L_p = 2700$ mm. (a) shear stress, (b) normal stress.

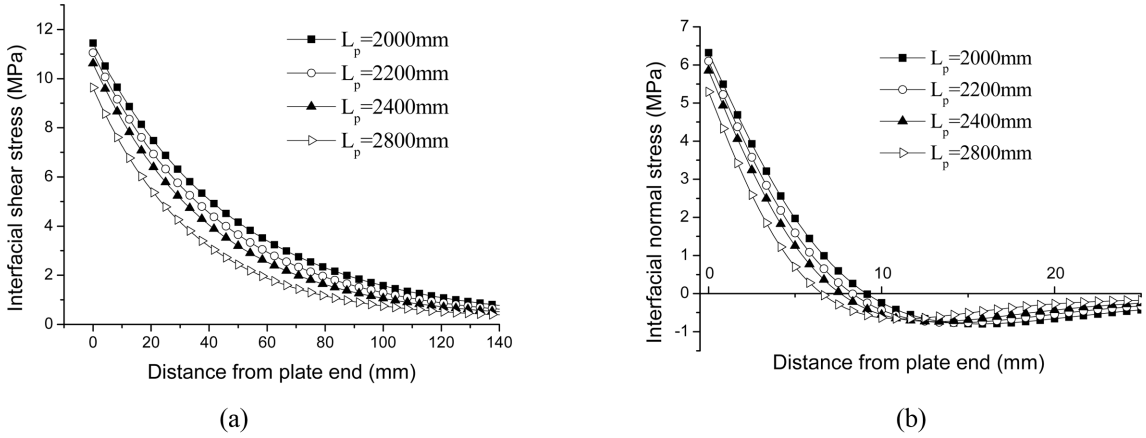

Fig. 11 The effect of plate thickness on interfacial stresses when $L_p = 2700$ mm. (a) shear stress, (b) normal stress

were found to be considerably influenced by the thickness of the plate. The results indicate that the maximum values of both the interfacial shear stress and the normal stress decrease with increased plate thickness. In addition, the maximum values of both normal and shear stresses decreased with increased plate length, as shown in Fig. 11. This figure shows the results when the length of the plate L_p was 2000, 2200, 2400, and 2800 mm for a constant thickness of h_p = 4 mm.

5.8 Impacts of thermal loads on interfacial stresses

The effects of the different temperature expansion coefficients for the beam and plate on interfacial stresses are discussed in section 5.5. However, not only are the adherends expanded by temperature elevation but the elastic modulus of commonly used epoxy adhesives may decrease significantly with increased temperature (Kelmar *et al*. 2008, Rabinovitch 2010). A high

Table 3 Temperature dependent elastic and shear moduli of the adhesive (adapted form Kelmar *et al.* (2008) and Rabinovitch (2010))

Temperature (°C)	20	30	40	50	60
E_a (MPa)	12800	12000	10400	6700	1000
G_a (MPa)	4925	4615	4000	2575	385

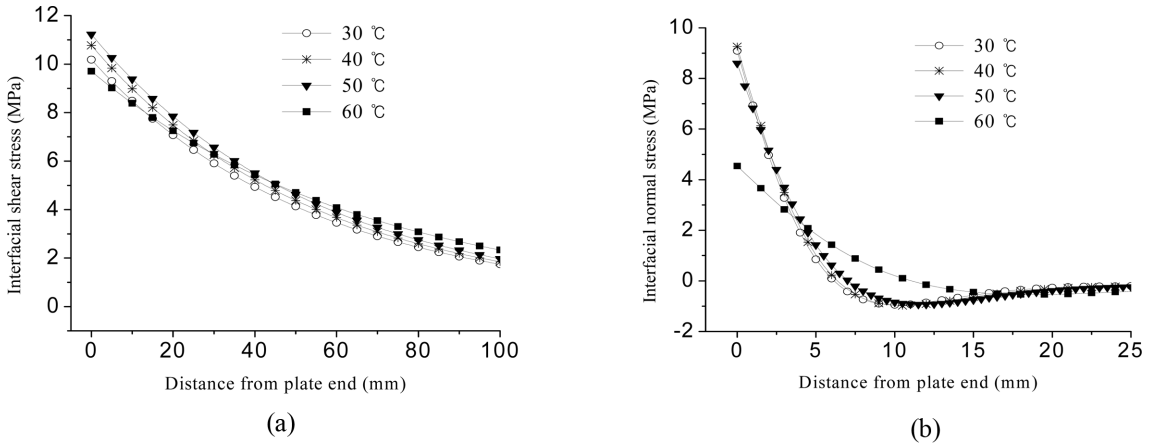

Fig.12 Impacts of thermal loads on interfacial stresses. (a) shear stress, (b) normal stress

temperature elevation (ΔT) was demonstrated to lead to a high stress concentration (see section 5.5), and a decrease in adhesive elastic modulus reduces the maximum values of both interfacial shear and normal stresses (see section 5.7.1). Thus, the impacts of thermal loads on the interfacial stress distribution were examined by simultaneously considering the thermal expansion of adherends and the change in adhesive elastic modulus induced by thermal loads.

Table 3 refers to Kelmar *et al.* (2008) and Rabinovitch (2010) to give the temperature-dependent elastic and shear moduli of the adhesive.

Fig. 12 shows the distribution of interfacial shear and normal stresses near the end of plate when the temperature is 30, 40, 50, and 60°C, assuming that the initial temperature is 20°C. It indicates an increase in interfacial shear stresses with increasing temperature when the temperature was 30–50°C. However, the interfacial normal stress is reduced by increasing the temperature to 50–60°C. Both the interfacial shear and normal stresses at the plate end clearly dropped when the temperature was 60°C because of a notable reduction in the elastic properties of the adhesive.

6. Conclusions

In this paper, we presented an improved solution for the interfacial stresses of a beam strengthened by bonding a plate onto its tension surface. The solution can be used to analyze plated beams that are simultaneously subjected to mechanical loads, prestressing, and thermal loads. The coupled equations for interfacial shear and normal stresses were derived by considering the curvature mismatch between the plate and beam induced by adhesive deformation. The new

analysis also includes the effect of the adherend shear deformations by assuming a parabolic variation of longitudinal displacements in both the beam and the bonded plate. The results indicated that incorporating the adherend shear deformation effects of the beam and plate clearly reduces the level of interfacial stress concentration. The curvature mismatch between the beam and the plate induces a small increase in interfacial stresses.

The main quantities that affect the distribution of interfacial stresses were analyzed. The maximum values of interfacial stresses at the end of the plate decrease with increased plate thickness and length. Moreover, increasing the thickness of the adhesive layer decreases the level and concentration of the interfacial stresses.

Both the normal and the shear stresses were demonstrated to be significantly influenced by the coupled effects of the elastic moduli, which appear as ratios E_a/E_b and E_a/E_p. Increasing E_a/E_b reduces interfacial stresses at the end of the plate, but increasing E_a/E_p induces higher interfacial stresses.

The difference in thermal expansion coefficients between the beam and the plate results in an increase in interfacial stress concentration when the temperature elevation (ΔT) is increased. In addition, an increase in the initial prestressing force (P_0) markedly increases the level of interfacial stress concentration. However, if the thermal expansion and variation in the elastic modulus of the adhesive with temperature are considered simultaneously, the interfacial shear stress near the plate end increases with increasing temperature when the temperature is 30-50°C. However, the interfacial normal stress is reduced by increasing the temperature to 50-60°C. Both the interfacial shear and the normal stresses clearly decrease when the temperature is 60°C because of a notable reduction in the elastic properties of the adhesive.

Acknowledgements

This work is supported by the National Natural Science Foundation of China (Grant No. 10802073) and 100 Excellent Talents Program in University of Hebei Province of China (CPRC019).

References

Ahmed, O., Van Gemert, D. and Vandewalle, L. (2001), "Improved model for plate-end shear of CFRP strengthened RC beams", *Cem. Concr. Compos.,* **23**, 3-19.

Arduini, M., Di-Tommaso, A. and Nanni, A. (1997), "Brittle failure in FRP plate and sheet bonded beams", *ACI Struct. J.,* **94**(4), 363-369.

Arslan, G., Sevuk, F. and Ekiz, I. (2008), "Steel plate contribution to load-carrying capacity of retrofitted RC beams", *Constr. Build. Mater.,* **22**, 143-153.

Ascione, L. and Feo, L. (2000), "Modelling of composite/concrete interface of RC beams strengthened with composite laminates", *Compos. Part B-Eng.,* **31**, 535-540.

Barnes, R.A. and Mays, G.C. (2001), "The transfer of stress through a steel to concrete adhesive bond", *Int. J. Adhes. Adhes.,* **21**, 495-502.

Benachour, A., Benyoucef, S., Tounsi, A. and Adda bedia, E.A. (2008), "Interfacial stress analysis of steel beams reinforced with bonded prestressed FRP plate", *Eng. Struct.,* **30**, 3305-3315.

Benyoucef, S., Tounsi, A., Meftah, S.A. and Adda Bedia, E.A. (2006), "Approximate analysis of the interfacial stress concentrations in FRP-RC hybrid beams", *Compos. Interfaces,* **13**(7), 561-571.

Bonacci, J.F. and Maalej, M. (2001), "Behavioral trends of RC beams strengthened with externally bonded

FRP", *J. Compos. Constr. ASCE,* **5**(2), 102-113.
Chen, J.F. and Teng, J.G. (2003), "Shear capacity of FRP-strengthened RC beams: FRP debonding", *Constr. Build. Mater.,* **17**, 27-41.
Deng, J., Lee, M.M.K. and Moy, S.S.J. (2004), "Stress analysis of steel beams reinforced with a bonded CFRP plate", *Compos. Struct.,* **65**, 205-215.
Etman, E.E. and Beeby, A.W. (2000), "Experimental program and analytical study of bond stress distributions on a composite plate bonded to a reinforced concrete beam", *Cement Concrete Compos.,* **22**, 281-291.
Fanning, P.J. and Kelly, O. (2001), "Ultimate response of RC beams strengthened with CFRP plates", *J. Compos. Constrt. ASCE,* **5**(2), 122-127.
Gao, B., Leung, C.K.Y. and Kim, J.K. (2005), "Prediction of concrete cover separation failure for RC beams strengthened with CFRP strips", *Eng. Struct.,* **27**(2), 177-189.
Garden, H.N., Quantrill, R.J., Hollaway, L.C., Thorne, A.M. and Parke, G.A.R. (1998), "An experimental study of the anchorage length of carbon fiber composite plates used to strengthen reinforced concrete beams", *Constr. Build. Mater.,* **12**, 203-219.
Hao, S.W., Li, Y.Y., Sun, J., Liu, Q., Wang, B. and Yang, H.Z. (2010), "A coupling solution for interfacial stresses in a plated beam", *J. Strain Anal. Eng.,* **45**(7), 513-521.
Jones, R., Swamy, R.N. and Charif, A. (1988), "Plate separation and anchorage of reinforced concrete beams strengthened by epoxy bonded steel plates", *Struct. Eng.,* **66**(5), 85-94.
Kelmar, E.L., Hordijk, D.A. and Hermes, M.C.J. (2008), "The influence of temperature on RC beams strengthened with externally bonded CFRP reinforcement", *Heron,* **53**(3), 157-185.
Maalej, M. and Bian, Y. (2001), "Interfacial shear stress concentration in FRP-strengthened beams", *Compos. Struct.,* **54**, 417-426.
Maalej, M. and Leong, K.S. (2005), "Effect of beam size and FRP thickness on interfacial shear stress concentration and failure mode of FRP-strengthened beams", *Compos. Sci. Technol.,* **65**, 1148-1158.
Malek, A.M., Saadatmanesh, H. and Ehsani, M.R. (1998), "Prediction of failure load of R/C beams strengthened with FRP plate due to stress concentration at the plate end", *ACI Struct. J.,* **95**(1), 142-152.
Oehlers, D.J. (1992), "Reinforced concrete beams with plates glued to their soffits", *J. Struct. Eng. ASCE,* **118**(8), 2023-2038.
Rabinovitch, O. (2010), "Impact of thermal loads on interfacial debonding in FRP strengthened beams", *Int. J. Solids Struct.,* **47**, 3234-3244.
Rabinovich, O. and Frostig, Y. (2000), "Closed-form high-order analysis of RC beams strengthened with FRP strips", *J. Compos. Constr. ASCE,* **4**(2), 65-74.
Rahimi, H. and Hutchinson, A. (2001), "Concrete beams strengthened with externally bonded FRP plates", *J. Compos. Constr. ASCE,* **5**(1), 44-56.
Raoof, M., El-Rimawi, J.A. and Hassanen, M.A.H. (2000), "Theoretical and experimental study on externally plated RC beams", *Eng. Struct.,* **22**, 85-101.
Rasheed, H.A. and Pervaiz, S. (2002), "Bond slip analysis of fiber-reinforced polymer-strengthened beams", *J. Eng. Mech.,* **128**, 78-86.
Roberts, T.M. (1989), "Approximate analysis of shear and normal stress concentrations in the adhesive layer of plated RC beams", *Struct. Eng.,* **67**(12), 229-233.
Roberts, T.M. and Haji-Kazemi, H. (1989), "A theoretical study of the behaviour of reinforced concrete beams strengthened by externally bonded steel plates", *P. I. Civil Eng. PT 2,* **87**, 39-55.
Saadatmanesh, H. and Ehsani, M.R. (1991), "RC beams strengthened with GFRP plates: I. Experimental study", *J. Struct. Eng. ASCE,* **117**(11), 3417-3433.
Schnerch, D., Dawood, M., Rizkalla, S. and Stamford, K. (2006), "Bond behavior of CFRP strengthened steel structures", *Adv. Struct. Eng.,* **9**(6), 805-817.
Shen, H.S., Teng, J.G. and Yang, J. (2001), "Interfacial stresses in beams and slabs bonded with a thin plate", *J. Eng. Mech. ASCE*, **127**(4), 399-406.
Smith, S.T. and Teng, J.G. (2002a), "FRP-strengthened RC beams. I: Review of debonding strength models", *Eng. Struct.,* **24**(4), 385-395.
Smith, S.T. and Teng, J.G. (2002b), "FRP-strengthened RC beams. II: Assessment of debonding strength models", *Eng. Struct.,* **24**(4), 397-417.

Smith, S.T. and Teng, J.G. (2001), "Interfacial stresses in plated beams", *Eng. Struct.,* **23**(7), 857-871.
Stratford, T. and Cadei, J. (2006), "Elastic analysis of adhesion stresses for the design of a strengthening plate bonded to a beam", *Constr. Build. Mater.,* **20**, 34-45.
Swamy, R.N., Jones, R. and Charif, A. (1989), "The effect of external plate reinforcement on the strengthening of structurally damaged RC beams", *Struct. Eng.,* **67**(3), 45-56.
Täljsten, B. (1997), "Strengthening of beams by plate bonding", *J. Mater. Civil. Eng. ASCE,* **9**(4), 206–212.
Teng, J.G., Zhang, J.W. and Smith, S.T. (2002), "Interfacial stresses in RC beams bonded with a soffit plate: a finite element study", *Constr. Build. Mater.,* **16**(1), 1-14.
Tounsi, A. (2006), "Improved theoretical solution for interfacial stresses in concrete beams strengthened with FRP plate", *Int. J. Solids Struct.,* **43**, 4154-4174.
Tounsi, A. and Benyoucef, S. (2007), "Interfacial stresses in externally FRP-plated concrete beams", *Int. J. Adhes. Adhes.,* **27**, 207-215.
Tounsi, A., Hassaine Daouadji, T., Benyoucef, S. and Addabedia, E.A. (2009), "Interfacial stresses in FRP-plated RC beams: Effect of adherend shear deformations", *Int. J. Adhes. Adhes.,* **29**, 343-351.
Tsai, M.Y., Oplinger, D.W. and Morton, J. (1998), "Improved theoretical solutions for adhesive lap joints", *Int. J. Solids Struct.,* **35**(12), 1163-1185.
Wang, J. (2006), "Debonding of FRP-plated reinforced concrete beam, a bond-slip analysis. I. Theoretical formulation", *Int. J. Solids Struct.,* **43**, 6649-6664.
Wang, J. and Zhang, C. (2010), "A three-parameter elastic foundation model for interface stresses in curved beams externally strengthened by a thin FRP plate", *Int. J. Solids Struct.,* **47**, 998-1006.
Yang, J., Chen, J.F. and Teng, J.G. (2009), "Interfacial stress analysis of plated beams under symmetric mechanical and thermal loading", *Constr. Build. Mater.,* **23**, 2973-2987.
Yang, J. and Wu, Y.F. (2007), "Interfacial stresses of FRP strengthened concrete beams: Effect of shear deformation", *Compos. Struct.,* **80**, 343-351.
Yang, J. and Ye, J. (2010), "An improved closed-form solution to interfacial stresses in plated beams using a two-stage approach", *Int. J. Mech. Sci.,* **52**, 13-30.
Yao, J. and Teng, J.G. (2007), "Plate end debonding in FRP-plated RC beams-I: Experiments", *Eng. Struct.,* **29**, 2457-2471.
Ziraba, Y.N. and Baluch, M.H. (1995), "Computational model for reinforced concrete beams strengthened by epoxy bonded steel plates", *Finite Elem. Anal. Des.,* **20**, 253-271.